AN INVESTIGATION OF SEVERAL NUMERICAL PROCEDURES FOR TIME-ASYMPTOTIC COMPRESSIBLE NAVIER-STOKES SOLUTIONS

By David H. Rudy, Dana J. Morris, Doris K. Blanchard,
NASA Langley Research Center

Charlie H. Cooke,
Old Dominion University

and Stanley G. Rubin
Polytechnic Institute of New York

SUMMARY

The status of an investigation of four numerical techniques for the time-dependent compressible Navier-Stokes equations is presented. Results for free shear layer calculations in the Reynolds number range from 10^3 to 8.1×10^4 indicate that a sequential alterating-direction implicit (ADI) finite-difference procedure requires longer computing times to reach steady state than a low-storage hopscotch finite-difference procedure. A finite-element method with cubic approximating functions was found to require excessive computer storage and computation times. A fourth method, an alternating-direction cubic spline technique which is still being tested, is also described.

INTRODUCTION

The quasi-parallel assumption successfully used in boundary-layer-type calculations is not applicable for many free mixing flows. The complete Navier-Stokes equations must usually be solved for flows which have no single dominant flow direction. This paper presents the current status of a detailed investigation of several numerical procedures for obtaining steady-state solutions for two-dimensional, high Reynolds number, compressible free shear flows using the time-asymptotic approach. In particular, the research has been directed toward the solution of mixed subsonic-supersonic flow problems.

Most published numerical solutions of the compressible viscous time-dependent Navier-Stokes equations have been for flows with Reynolds numbers much less than 10^3. Peyret and Viviand (ref. 1) have summarized these solutions through mid-1973. Taylor (ref. 2) also analyzed the literature at that time. Most methods up to the time of these surveys used explicit difference schemes. Later, Briley and McDonald (ref. 3) and Baum and Ndefo (ref. 4) published alternating-direction implicit (ADI) calculations. The high Reynolds number solutions (Victoria and Steiger (ref. 5), Carter (ref. 6), and MacCormack (ref. 7)) were all computed with explicit difference schemes. Recently, additional high Reynolds number solutions have appeared, e.g., Holst and Tannehill (ref. 8) and Baldwin and MacCormack (ref. 9). These solutions were also computed with explicit methods.

Although conceptually simpler and more easily coded than implicit methods, explicit methods are restricted to small time steps relative to the spatial grid size for numerical stability. Consequently, such methods require long computation times to reach a steady state, especially for flows in which a fine mesh has been used such as in regions of high shear. For example, the calculation of a shear layer impinging on a blunt body for a Reynolds number of 10^4 by Holst, Tannehill, and Rakich (ref. 10) using the MacCormack method requires up to 80 min on a CDC 7600 computer.

The methods under investigation are the following: (1) hopscotch (explicit) finite difference, (2) alternating-direction implicit (ADI) finite difference, (3) finite element, and (4) implicit cubic spline integration. In addition, some calculations have been made with the Du Fort-Frankel procedure. The goal of this study is the development of an efficient numerical tool to be used in testing fully two-dimensional turbulence models for a wide range of free shear flow applications such as interference heating (shock/shear layer impingement), separated flows, jet exhaust noise reduction, combustor design, and tangential slot injection. This paper summarizes results of calculations for sample mixing problems with Reynolds numbers ranging from 10^3 to 8.1×10^4. The procedures are compared with respect to their accuracy, computer storage requirements, ease of implementation, and total time to steady state for computation of sample problems.

SYMBOLS

c	speed of sound
D_j	diameter of jet
f,g	general functions
H	enthalpy
L	differential operator
M	Mach number
M_i	second derivative of $S(x_i)$

m_i	first derivative of $S(x_i)$
N	integer
N_{Co}	Courant number, $\frac{\Delta t}{\Delta x/(u + v + 2c)}$
N_{Re}	Reynolds number, $\frac{\bar{\rho}_s \bar{u}_{ref} D_j}{\bar{\mu}_s}$
p	pressure
R	gas constant
$S(x)$	cubic spline function
T	temperature
t	time
u	streamwise velocity
u_{ref}	reference velocity, $\sqrt{2\bar{H}_s}$
V	vector of unknowns
v	normal velocity
x,y	streamwise and normal directions, respectively
α	artificial diffusion coefficient
γ	ratio of specific heats
Δ	incremental change
μ	molecular viscosity
ν	kinematic viscosity
ρ	density

ϕ_J	B-spline function in equation (14)

Subscripts:

i,j	index denoting grid point spatial location
J	nodal index in finite-element mesh
s	stagnation condition
t,x,y	derivative with respect to time, x-direction, and y-direction

Superscripts:

n,*	index denoting time level

A bar over a symbol denotes a dimensional quantity. An arrow over a symbol denotes a vector quantity.

PROBLEM DEFINITION

To provide a basis for comparison of the numerical procedures, a set of standard test problems was selected.

Sample Problems

Figure 1(a) shows the mixing problem (case 1) originally chosen for use as the standard sample problem. This flow is the mixing of a two-dimensional laminar supersonic (Mach 3) jet and a laminar subsonic flow normal to the jet axis. The peripheral velocity v_p is higher in magnitude than the normal velocity component arising from natural entrainment of the resultant free shear layer for the same jet issuing into quiescent surroundings. As shown in figure 1(a), the solution domain does not extend to infinity in either the positive streamwise or normal directions. The peripheral flow is applied one or more jet diameters above the corner of the wall, and the calculation is truncated one jet diameter downstream from the jet exit plane. This problem thus embodies some complicating factors which are often unavoidable in computations of flow fields for real vehicles, e.g., a sharp corner and the artificial downstream boundary with a significant portion of subsonic outflow. Since the individual effects of these factors are difficult to isolate in the computation of such a flow field, calculations were also made for the related problem, mixing of two parallel streams, shown in figure 1(b). The computational region begins downstream of the base of the infinitely thin splitter plates. Such a calculation obviously does not require the full Navier-Stokes equations, since solutions can be obtained with the usual quasi-parallel approach (boundary-layer equations with free shear flow boundary conditions). However, since steady-state calculations could be made with another method, solutions were obtained for comparison with computed Navier-Stokes results. The mixing of a subsonic stream and a supersonic stream (case 2) shown in figure 1(b) was chosen for the study of subsonic boundary conditions. Calculations were also made for the mixing of two supersonic (Mach 3 and Mach 1.68) streams (case 3), a flow free from subsonic boundary problems.

Governing Equations

The governing equations can be written in nonconservative forms as follows:

Continuity

$$\rho_t + \rho v_y + \rho u_x + v\rho_y + u\rho_x = 0 \tag{1}$$

x-momentum

$$\rho u_t + \rho v u_y + \rho u u_x = -p_x + \frac{4}{3N_{Re}}\left(\mu u_x\right)_x - \frac{2}{3N_{Re}}\left(\mu v_y\right)_x + \frac{1}{N_{Re}}\left[\mu\left(u_y + v_x\right)\right]_y \tag{2}$$

y-momentum

$$\rho v_t + \rho v v_y + \rho u v_x = -p_y + \frac{4}{3N_{Re}}\left(\mu v_y\right)_y - \frac{2}{3N_{Re}}\left(\mu u_x\right)_y + \frac{1}{N_{Re}}\left[\mu\left(u_y + v_x\right)\right]_y \tag{3}$$

These equations are nondimensionalized with respect to the jet diameter and stagnation flow conditions, i.e.,

$$\rho = \frac{\bar{\rho}}{\bar{\rho}_s} \qquad p = \frac{\bar{p}}{2\bar{\rho}_s\bar{H}_s}$$

$$T = \frac{\bar{T}}{\bar{T}_s} \qquad x = \frac{\bar{x}}{D_j}$$

$$\bar{u}_{ref} = \sqrt{2\bar{H}_s} \qquad y = \frac{\bar{y}}{D_j}$$

$$u = \frac{\bar{u}}{\sqrt{2\bar{H}_s}} = \frac{\bar{u}}{\bar{u}_{ref}} \qquad N_{Re} = \frac{\bar{\rho}_s\bar{u}_{ref}D_j}{\bar{\mu}_s}$$

$$v = \frac{\bar{v}}{\sqrt{2\bar{H}_s}} = \frac{\bar{u}}{\bar{u}_{ref}} \qquad \mu = \frac{\bar{\mu}}{\bar{\mu}_s}$$

The pressure was evaluated by means of the perfect gas equation of state

$$p = \rho RT \tag{4}$$

where $R = \frac{\gamma - 1}{2\gamma}$. Air was the test gas. Only laminar (molecular) viscous effects were considered, the Sutherland law being used to express the viscosity as a function of temperature

$$\mu = T^{3/2} \frac{1 + 198.6/\overline{T}_s}{T + 198.6/\overline{T}_s} \tag{5}$$

To simplify the system of governing equations and to reduce required machine storage, a constant total temperature of 530° R (294 K) was assumed. Calculations for a Mach 3 jet into still air with the quasi-parallel code of Oh (ref. 11), which included the energy equation, showed that the total enthalpy varied less than 5 percent throughout the mixing region from the constant value assumed in other calculations. This small variation had a negligible effect on the other flow parameters. As a result of this assumption, the temperature could be evaluated by the algebraic relationship

$$T = 1 - u^2 - v^2 \tag{6}$$

which eliminated the need for solving the complete energy equation. Constant static pressure was assumed in all calculations to generate initial values of density using equations (4) and (6) along with the given initial velocities. The linearized version of equations (1) to (6) with the viscous terms neglected has been shown by Gottlieb and Gustafsson (ref. 12) to be well-posed for the initial value problem.

DESCRIPTION OF NUMERICAL PROCEDURES

Hopscotch

The hopscotch method is a two-step explicit procedure which was shown to be unconditionally stable for the diffusion equation by Gourlay (ref. 13). It was used by Scala and Gordon (ref. 14) for compressible viscous calculations of low Reynolds number flow around a circular cylinder, and it has been applied to hyperbolic systems with shocks by Gourlay and Morris (ref. 15).

Figure 2 shows the pattern of the two sweeps. Consider, for example, the equation

$$u_t = u_{xx} + u_{yy} \tag{7}$$

With forward time and centered space differencing, $u_{i,j}^{n+1}$ is computed at each time step at the nodes for which $i + j + n$ is even (marked with circles in fig. 2) during the first sweep through the mesh with the equation

$$u_{i,j}^{n+1} = u_{i,j}^{n} + \Delta t\left[\frac{u_{i+1,j}^{n} - 2u_{i,j}^{n} + u_{i-1,j}^{n}}{(\Delta x)^2}\right] + \Delta t\left[\frac{u_{i,j+1}^{n} - 2u_{i,j}^{n} + u_{i,j-1}^{n}}{(\Delta y)^2}\right] \tag{8}$$

This sweep is fully explicit. In the second sweep at this time step,

$$u_{i,j}^{n+1} = u_{i,j}^{n} + \Delta t\left[\frac{u_{i+1,j}^{n+1} - 2u_{i,j}^{n+1} + u_{i-1,j}^{n+1}}{(\Delta x)^2}\right] + \Delta t\left[\frac{u_{i,j+1}^{n+1} - 2u_{i,j}^{n+1} + u_{i,j-1}^{n+1}}{(\Delta y)^2}\right] \tag{9}$$

at the nodes (marked with squares in fig. 2) for which $i + j + n$ is odd. This sweep is implicit in the sense that the values in the computation of the spatial derivatives are at the new time level $n + 1$. However, this implicitness does not require the reduction of a matrix, since these values were computed during the first sweep. Differencing which does not fit into this pattern, such as a five-point difference for u_{xx} using values of $u_{i+2,j}^{n+1}$ and $u_{i-2,j}^{n+1}$, requires special consideration. The conventional nine-point difference analog for cross-derivative terms must receive treatment which usually requires the reduction of a matrix. The computational efficiency of the hopscotch procedure is thus reduced. For the full Navier-Stokes equations, hopscotch has no cell Reynolds number limitation, but the maximum time step is limited by the condition, $\Delta t \leq \frac{\Delta x}{u + v + 2c}$. For the present application, a sufficient condition for stability is $\Delta t \leq \frac{\Delta x}{u + v + \sqrt{2}c}$.

The hopscotch version derived for the present investigation is a low-storage procedure (one array per dependent variable). The equations were linearized by lagging the nonlinear coefficients. On the second sweep, values at time $n + 1$ are used only where available. This lagging eliminates the need for matrix reductions and thereby simplifies the coding, maintains the low storage, and minimizes CPU time per nodal point. Gottlieb and Gustafsson (ref. 12), considering the convective terms only, have analyzed the stability of this version of hopscotch with the lagging of some values and have found its stability to be identical to that of the original hopscotch method. The method is different, however, when the diffusion terms are included. The stability limit which was derived from the advection terms is not changed for the range of Reynolds number considered in the present investigation. The lagging of values used to compute the viscous terms introduces slightly more second-order dissipation than in the original hopscotch method. The new procedure is formally not consistent with the time-dependent problem; however, the extra error term introduced is very small for large Reynolds numbers (such as 10^3). In the present application the interest is not in the transient but in the steady-state solution; therefore, this error term, which goes to zero at steady state, has no detrimental effect.

During each sweep the x-momentum, y-momentum, and continuity equations are solved sequentially at each nodal point with the boundary values then being updated at the end of each time step. To illustrate the present version of hopscotch, the differencing of the x-momentum equation is as follows:

First sweep

$$
\begin{aligned}
u_{i,j}^{n+1} = u_{i,j}^{n} + \Delta t \Bigg\{ & -u_{i,j}^{n}\left(\frac{\partial u}{\partial x}\right)_{i,j}^{n} - v_{i,j}^{n}\left(\frac{\partial u}{\partial y}\right)_{i,j}^{n} - \frac{1}{\rho_{i,j}^{n}}\left(\frac{\partial p}{\partial x}\right)_{i,j}^{n} \\
& + \frac{4}{3N_{Re}\rho_{i,j}^{n}}\Bigg[2A\left(\frac{\mu_{i+1,j}^{n} + \mu_{i,j}^{n}}{2}\right)\left(\frac{u_{i+1,j}^{n} - u_{i,j}^{n}}{\Delta x_i}\right) + 2B\mu_{i,j}^{n}\left(\frac{\partial u}{\partial x}\right)_{i,j}^{n} \\
& + 2C\left(\frac{\mu_{i,j}^{n} + \mu_{i-1,j}^{n}}{2}\right)\left(\frac{u_{i,j}^{n} - u_{i-1,j}^{n}}{\Delta x_{i-1}}\right)\Bigg] - \frac{2}{3N_{Re}\rho_{i,j}^{n}}\Bigg[A\mu_{i+1,j}^{n}\left(\frac{\partial v}{\partial y}\right)_{i+1,j}^{n} + B\mu_{i,j}^{n}\left(\frac{\partial v}{\partial y}\right)_{i,j}^{n} \\
& + C\mu_{i-1,j}^{n}\left(\frac{\partial v}{\partial y}\right)_{i-1,j}^{n}\Bigg] + \frac{1}{N_{Re}\rho_{i,j}^{n}}\Bigg[2D\left(\frac{\mu_{i,j+1}^{n} + \mu_{i,j}^{n}}{2}\right)\left(\frac{u_{i,j+1}^{n} - u_{i,j}^{n}}{\Delta y_j}\right) + 2E\mu_{i,j}^{n}\left(\frac{\partial u}{\partial y}\right)_{i,j}^{n} \\
& + 2F\left(\frac{\mu_{i,j}^{n} + \mu_{i,j-1}^{n}}{2}\right)\left(\frac{u_{i,j}^{n} - u_{i,j-1}^{n}}{\Delta y_{j-1}}\right)\Bigg] + \frac{1}{N_{Re}\rho_{i,j}^{n}}\Bigg[D\mu_{i,j+1}^{n}\left(\frac{\partial v}{\partial x}\right)_{i,j+1}^{n} \\
& + E\mu_{i,j}^{n}\left(\frac{\partial v}{\partial x}\right)_{i,j}^{n} + F\mu_{i,j-1}^{n}\left(\frac{\partial v}{\partial x}\right)_{i,j-1}^{n}\Bigg]\Bigg\}
\end{aligned}
\tag{10}
$$

where A, B, C, D, E, and F are coefficients arising from the differencing.

Second sweep

$$
u_{i,j}^{n+1} = u_{i,j}^{n} + \Delta t \Bigg\{ - u_{i,j}^{n}\left(\frac{\partial u}{\partial x}\right)_{i,j}^{n+1} - v_{i,j}^{n}\left(\frac{\partial v}{\partial y}\right)_{i,j}^{n+1} - \frac{1}{\rho_{i,j}^{n}}\left(\frac{\partial p}{\partial x}\right)_{i,j}^{n+1}
$$

(Equation continued on next page)

$$
\begin{aligned}
&+ \frac{4}{3N_{Re}\rho^{n}_{i,j}}\Bigg[2A\left(\frac{\mu^{n+1}_{i+1,j} + \mu^{n}_{i,j}}{2}\right)\left(\frac{u^{n+1}_{i+1,j} - u^{n}_{i,j}}{\Delta x_{i}}\right) + 2B\mu^{n}_{i,j}\left(\frac{\partial u}{\partial x}\right)^{n+1}_{i,j} \\
&+ 2C\left(\frac{\mu^{n}_{i,j} + \mu^{n+1}_{i-1,j}}{2}\right)\left(\frac{u^{n}_{i,j} - u^{n+1}_{i-1,j}}{\Delta x_{i-1}}\right)\Bigg] - \frac{2}{3N_{Re}\rho^{n}_{i,j}}\Bigg[A\mu^{n+1}_{i+1,j}\left(\frac{\partial v}{\partial y}\right)^{n+1}_{i+1,j} + B\mu^{n}_{i,j}\left(\frac{\partial v}{\partial y}\right)^{n+1}_{i,j} \\
&+ C\mu^{n+1}_{i-1,j}\left(\frac{\partial v}{\partial y}\right)^{n+1}_{i-1,j}\Bigg] + \frac{1}{N_{Re}\rho^{n}_{i,j}}\Bigg[2D\left(\frac{\mu^{n+1}_{i,j+1} + \mu^{n}_{i,j}}{2}\right)\left(\frac{u^{n+1}_{i,j+1} - u^{n}_{i,j}}{\Delta y_{j}}\right) + 2E\mu^{n}_{i,j}\left(\frac{\partial u}{\partial y}\right)^{n+1}_{i,j} \\
&+ 2F\left(\frac{\mu^{n}_{i,j} + \mu^{n+1}_{i,j-1}}{2}\right)\left(\frac{u^{n}_{i,j} - u^{n+1}_{i,j-1}}{\Delta y_{j-1}}\right)\Bigg] + \frac{1}{N_{Re}\rho^{n}_{i,j}}\Bigg[D\mu^{n+1}_{i,j+1}\left(\frac{\partial v}{\partial x}\right)^{n+1}_{i,j+1} \\
&+ E\mu^{n}_{i,j}\left(\frac{\partial v}{\partial x}\right)^{n+1}_{i,j} + F\mu^{n+1}_{i,j-1}\left(\frac{\partial v}{\partial x}\right)^{n+1}_{i,j-1}\Bigg]\Bigg\}
\end{aligned}
\tag{11}
$$

Alternating-Direction Implicit Method

The alternating-direction implicit (ADI) technique developed by Peaceman and Rachford (ref. 16) is a two-step procedure requiring reduction of tridiagonal matrices for which an efficient solution algorithm, the Thomas algorithm (ref. 17), exists. The method was originally applied to the two-dimensional heat conduction equation in reference 16 and later to a system of hyperbolic equations by Gourlay and Mitchell (ref. 18). For both of these model problems, it was shown to possess unconditional stability. The method, however, has not been extensively applied to the compressible Navier-Stokes equations. In 1966, Polezhaev (ref. 19) obtained solutions for a natural convection problem. His ADI method removed the diffusion time-step limitation; however, he found experimentally that the time step was still limited to the usual maximum explicit value. In 1973, Baum and Ndefo (ref. 4) published a two-dimensional implicit method based on the Peaceman-Rachford procedure. The Baum-Ndefo method iteratively solves nonlinear difference equations as a sequence of linear equations using a quasi-linearization technique. In a one-dimensional calculation of shock structure, the method was found to be stable for Courant numbers as large as 10. However, reference 4 does not consider the full Navier-Stokes equations. Later in 1973, Briley and McDonald (ref. 3) presented a method based on a fully implicit backward time difference scheme in which nonlinearities at the implicit time level are linearized by a Taylor's series expansion about the known time level. The resulting system of multidimensional coupled linear difference equations is solved with a noniterative Douglas-Gunn ADI approach. The method was shown to be stable for very large Courant numbers in calculation of three-dimensional subsonic flow in a straight duct with rectangular cross section. For a flow with Mach number of 0.044 and a Reynolds number of 60, stable solutions were obtained for Courant numbers up to 1250. For a Mach number of 0.5 and a Reynolds number of 600, the time step was gradually increased as the solution progressed, resulting in an average Courant number of 73. Thus, the actual Courant number decreases with increasing Reynolds number, perhaps because of diagonal dominance problems as discussed in reference 3. The computational effort per time step was reported to be twice that of most explicit methods.

In the ADI procedure used in the present investigation, a sequential solution of the difference equations is obtained for each row during the first one-half time step (horizontal sweep) and for each column during the second one-half time step (vertical sweep). All spatial derivatives were approximated by centered finite differences; time derivatives, by backward differences. The nonlinear coefficients in the convective terms were lagged one-half time step. In addition, the pressure terms and cross-derivative terms were treated explicitly in each sweep. The temperature and viscosity were updated for the entire field after each sweep. The order of solution for each row and column is (1) x-momentum equation, (2) y-momentum equation, and (3) continuity equation. The solution is then marched to steady state without iteration. This ADI formulation requires two storage arrays for u, v, ρ, and μ and one for T.

To illustrate the ADI method, the finite-difference form of the x-momentum equation is shown. For the horizontal sweep, from time level n to an intermediate time denoted by *,

$$\begin{aligned}
&\rho^n_{i,j}\left(\frac{u^*_{i,j} - u^n_{i,j}}{\Delta t/2}\right) + \rho^n_{i,j}v^n_{i,j}\left(\frac{u^n_{i,j+1} - u^n_{i,j-1}}{2\,\Delta y}\right) + \rho^n_{i,j}u^n_{i,j}\left(\frac{u^*_{i+1,j} - u^*_{i-1,j}}{2\,\Delta x}\right) \\
&\quad = -\left(\frac{p^n_{i+1,j} - p^n_{i-1,j}}{2\,\Delta x}\right) + \frac{1}{N_{Re}\,\Delta y}\left[\left(\frac{\mu^n_{i,j+1} + \mu^n_{i,j}}{2}\right)\left(\frac{u^n_{i,j+1} - u^n_{i,j}}{\Delta y}\right)\right. \\
&\qquad \left. - \left(\frac{\mu^n_{i,j} + \mu^n_{i,j-1}}{2}\right)\left(\frac{u^n_{i,j} - u^n_{i,j-1}}{\Delta y}\right)\right] + \frac{1}{N_{Re}\,\Delta y}\left[\mu^n_{i,j+1}\left(\frac{v^n_{i+1,j+1} - v^n_{i-1,j+1}}{2\,\Delta x}\right)\right. \\
&\qquad \left. - \mu^n_{i,j-1}\left(\frac{v^n_{i+1,j-1} - v^n_{i-1,j-1}}{2\,\Delta x}\right)\right] + \frac{4}{3N_{Re}\,\Delta x}\left[\left(\frac{\mu^n_{i+1,j} + \mu^n_{i,j}}{2}\right)\left(\frac{u^*_{i+1,j} - u^*_{i,j}}{\Delta x}\right)\right.
\end{aligned}$$

(Equation continued on next page)

$$-\left(\frac{\mu^{n}_{i,j}+\mu^{n}_{i-1,j}}{2}\right)\left(\frac{u^{*}_{i,j}-u^{*}_{i-1,j}}{\Delta x}\right)\Bigg] - \frac{2}{3N_{Re}\;\Delta x}\Bigg[\mu^{n}_{i+1,j}\left(\frac{v^{n}_{i+1,j+1}-v^{n}_{i+1,j-1}}{2\;\Delta y}\right)$$

$$-\mu^{n}_{i-1,j}\left(\frac{v^{n}_{i-1,j+1}-v^{n}_{i-1,j-1}}{2\;\Delta y}\right)\Bigg] \tag{12}$$

The unknowns are $u^{*}_{i-1,j}$, $u^{*}_{i,j}$, and $u^{*}_{i+1,j}$. Similarly, for the vertical sweep, from * to n+1,

$$\rho^{*}_{i,j}\left(\frac{u^{n+1}_{i,j}-u^{*}_{i,j}}{\Delta t/2}\right)+\rho^{*}_{i,j}v^{*}_{i,j}\left(\frac{u^{n+1}_{i,j+1}-u^{n+1}_{i,j-1}}{2\;\Delta y}\right)+\rho^{*}_{i,j}u^{*}_{i,j}\left(\frac{u^{*}_{i+1,j}-u^{*}_{i-1,j}}{2\;\Delta x}\right)$$

$$=-\left(\frac{p^{*}_{i+1,j}-p^{*}_{i-1,j}}{2\;\Delta x}\right)+\frac{1}{N_{Re}\;\Delta y}\Bigg[\left(\frac{\mu^{*}_{i,j+1}+\mu^{*}_{i,j}}{2}\right)\left(\frac{u^{n+1}_{i,j+1}-u^{n+1}_{i,j}}{\Delta y}\right)$$

$$-\left(\frac{\mu^{*}_{i,j}+\mu^{*}_{i,j-1}}{2}\right)\left(\frac{u^{n+1}_{i,j}-u^{n+1}_{i,j-1}}{\Delta y}\right)\Bigg]+\frac{1}{N_{Re}\;\Delta y}\Bigg[\mu^{*}_{i,j+1}\left(\frac{v^{*}_{i+1,j+1}-v^{*}_{i-1,j+1}}{2\;\Delta x}\right)$$

$$-\mu^{*}_{i,j-1}\left(\frac{v^{*}_{i+1,j-1}-v^{*}_{i-1,j-1}}{2\;\Delta x}\right)\Bigg]+\frac{4}{3N_{Re}\;\Delta x}\Bigg[\left(\frac{\mu^{*}_{i+1,j}+\mu^{*}_{i,j}}{2}\right)\left(\frac{u^{*}_{i+1,j}-u^{*}_{i,j}}{\Delta x}\right)$$

$$-\left(\frac{\mu^{*}_{i,j}+\mu^{*}_{i-1,j}}{2}\right)\left(\frac{u^{*}_{i,j}-u^{*}_{i-1,j}}{\Delta x}\right)\Bigg]-\frac{2}{3N_{Re}\;\Delta x}\Bigg[\mu^{*}_{i+1,j}\left(\frac{v^{*}_{i+1,j+1}-v^{*}_{i+1,j-1}}{2\;\Delta y}\right)$$

$$-\mu^{*}_{i-1,j}\left(\frac{v^{*}_{i-1,j+1}-v^{*}_{i-1,j-1}}{2\;\Delta y}\right)\Bigg] \tag{13}$$

Finite-Element Method

The finite-element method has been used extensively for the numerical solution of structural mechanics problems for a number of years; however, the procedure has only recently been applied to fluid mechanics problems. (See pp. 240-257 of ref. 20.) Using a stream-function—vorticity approach with linear elements, Baker (ref. 21) has developed an algorithm for steady viscous compressible flows. Solutions have been obtained for Reynolds numbers up to 7750. The present method appears to be the first finite-element procedure for the compressible Navier-Stokes equations in primitive variables.

The solution algorithm uses a Galerkin method with leapfrog time integration. The solution domain is discretized with triangular elements with bicubic trial functions. Figure 3 shows a finite-element mesh for case 1. As an example of a trial function, the density is of the form

$$\rho(x,y,t) = \sum_{J=1}^{10} \rho_J(t)\,\phi_J(x,y) \tag{14}$$

where J is the nodal index and the ϕ_J are the so-called B-spline basis functions which are piecewise cubic over the problem domain.

The unknown parameters in each trial function are the flow variable function values (ρ, u, and v) and their first partial derivatives $\left(\rho_x,\ \rho_y,\ u_x,\ u_y,\ v_x, \text{ and } v_y\right)$ at the triangle vertices and the function values alone at the triangle centroid. In the Galerkin approach, the weighted residuals formed by using the weights ϕ_J are set equal to zero. This yields a set of algebraic equations for the nodal values. Thus, if the governing equations are of the form

$$L(\omega) = 0$$

where ω is a general function, the Galerkin approach yields a set of equations

$$\iint\limits_{\substack{\text{Solution}\\ \text{domain}}} \phi_J(\omega) = 0 \tag{15}$$

The time discretization scheme is similar to the Crank-Nicolson Galerkin method described by Douglas and Dupont (ref. 22). Centered time differences over two time steps, $n - 1$ to $n + 1$, and the averaging of space derivatives over times $n - 1$ and $n + 1$ yield second-order time truncation error. This spatial averaging also eliminates nonlinearities in the resulting implicit system of difference equations. The system of determining equations has the following form:

Continuity

$$D^n \vec{\rho}^{\,n+1} = \overrightarrow{FD}^{n,n-1} \tag{16}$$

Momentum equations

$$\begin{bmatrix} ZZ & ZR \\ RZ & RR \end{bmatrix}^{n} \begin{Bmatrix} \vec{u} \\ \vec{v} \end{Bmatrix}^{n+1} = \begin{Bmatrix} \overrightarrow{FU} \\ \overrightarrow{FV} \end{Bmatrix}^{n,n-1} \tag{17}$$

where $\vec{\rho}$ is the unknown density vector, $\vec{u}$ and $\vec{v}$ are vectors of unknowns from the x- and y-momentum equations, ZZ, ZR, RZ, RR, and D are nonsymmetric matrices with varying bandwidth, and $\overrightarrow{FD}$, $\overrightarrow{FU}$, and $\overrightarrow{FV}$ are vectors of known quantity.

The matrices in these equations are assembled at each time step. The continuity equation is solved with a standard triangular decomposition method which takes advantage of matrix sparseness. The momentum equations are solved with a unique block iterative LU solver developed during the present investigation. Despite large matrices and the accompanying problem of efficient data management, the use of cubic elements yields fourth-order spatial discretization error. Cubic elements also allow exact incorporation of first-derivative boundary conditions, unlike finite-difference methods which require a discretization. In addition, the triangular mesh allows the method to be easily adapted to nonrectangular solution domains.

Cubic Spline Integration Method

The potential of a cubic spline collocation procedure for the numerical solution of partial differential equations has been demonstrated by Rubin and Graves (ref. 23) for several model problems. This use of a cubic spline approximation for the evaluation of spatial gradients provides a highly efficient and accurate procedure for computation with a nonuniform mesh (which is necessary for high Reynolds number calculations in the physical plane) and/or curvilinear boundaries. The basic spline approximation leads to a second-order accurate expression for second derivatives, e.g., the diffusion terms in the momentum equations, for both a uniform mesh and an arbitrarily nonuniform mesh. First derivatives, i.e., the convective terms, are third-order accurate with a nonuniform mesh and fourth-order accurate with a uniform mesh. With a three-point finite-difference approximation, the order of the truncation error is significantly decreased with even a moderate variation in the mesh spacing (ref. 24). Thus, the spline procedure is more accurate than the usual finite-difference procedures for nonuniform grids. The spline method also allows accurate interpolation if grid realinement becomes necessary.

In addition, first- and second-derivative boundary conditions can be applied more accurately and more easily than with conventional finite-difference methods, since discretization is unnecessary. Unlike the finite-element or other Galerkin procedures, the evaluation of quadratures, which are generally not tridiagonal, is unnecessary.

In reference 23, Rubin and Graves present a detailed discussion of the general spline formulation and methodology for solving second-order quasi-linear partial differential equations. Therefore, only a brief description of the general cubic spline procedure is presented in this paper.

A cubic spline $S(x)$ is a continuous function which has continuous first and second derivatives on an interval $a < x < b$ (a and b are two arbitrary points) and corresponds to a cubic polynomial in each subinterval $x_{i-1} \leq x \leq x_i$. The mesh spacing h_i is defined by $h_i = x_i - x_{i-1}$.

The following tridiagonal formulas are obtained by enforcing the continuity requirements at the collocation points x_i:

$$\frac{h_i}{6} M_{i-1} + \frac{h_i + h_{i+1}}{3} M_i + \frac{h_{i+1}}{6} M_{i+1} = \frac{u_{i+1} - u_i}{h_{i+1}} - \frac{u_i - u_{i-1}}{h_i} \tag{18}$$

$$\frac{1}{h_i} m_{i-1} + 2\left(\frac{1}{h_i} + \frac{1}{h_{i+1}}\right) m_i + \frac{1}{h_{i+1}} m_{i+1} = \frac{3\left(u_{i+1} - u_i\right)}{h_{i+1}^2} + \frac{3\left(u_i - u_{i-1}\right)}{h_i^2} \tag{19}$$

where at $x = x_i$, $S\left(x_i\right) = u_i$, $S'\left(x_i\right) = m_i$, and $S''\left(x_i\right) = M_i$. The following useful relationships also exist between the first and second derivatives:

$$m_{i+1} - m_i = \frac{h_{i+1}}{2}\left(M_i + M_{i+1}\right) \tag{20}$$

$$m_i = \frac{h_i}{3} M_i + \frac{h_i}{6} M_{i-1} + \frac{u_i - u_{i-1}}{h_i} \tag{21}$$

$$m_i = -\frac{h_{i+1}}{3} M_i - \frac{h_{i+1}}{6} M_{i+1} + \frac{u_{i+1} - u_i}{h_{i+1}} \tag{22}$$

For a governing partial differential equation of the form

$$u_t = f\left(u, u_x, u_{xx}\right) \tag{23}$$

the approximate solution is found by considering the solution of

$$\left(u_t\right)_i = f\left(u_i, m_i, M_i\right) \tag{24}$$

where the time derivative is discretized in the usual finite-difference manner, i.e.,

$$\left(u_t\right)_i = \frac{u_i^{n+1} - u_i^n}{\Delta t} \tag{25}$$

As an example, consider an implicit solution of the linearized Burgers' equation, which has the general form of the momentum equations

$$u_t + uu_x = \nu u_{xx} \tag{26}$$

where

$$u = u(x,t) \qquad \nu = \nu(x,t)$$

The approximation for this equation becomes

$$u_i^{n+1} = u_i^n - \Delta t\left(u_i^{n+1} m_i^{n+1}\right) + \Delta t\left(\nu_i^{n+1} M_i^{n+1}\right) \tag{27}$$

With the spline relations (18) and (19), a system of 3N equations is generated for 3(N + 2) unknowns. This system can be written as

$$A_i \vec{V}_{i-1}^{n+1} + B_i \vec{V}_i^{n+1} + C_i \vec{V}_{i+1}^{n+1} = D_i \vec{V}_i^n \tag{28}$$

where $\vec{V}_i = \left[u_i, m_i, M_i\right]^T$ and A, B, C, and D are 3 × 3 coefficient matrices. Initial conditions are prescribed so that $u(x,0) = g(x)$. Equations (20) to (22) can be used, if necessary, to relate information at the boundaries and provide a closed system which can then be solved by the standard tridiagonal algorithm.

An alternate procedure can be derived by substituting u_i and m_i as functions of M_i. The resulting tridiagonal system for M_i has the form

$$a_i M_{i-1}^{n+1} + b_i M_i^{n+1} + c_i M_{i+1}^{n+1} = d_i \qquad (i = 1, \ldots, N) \tag{29}$$

This procedure is being used in the present application for the two momentum equations. If the partial differential equation to be solved has no second-derivative terms (e.g., the continuity equation), a tridiagonal system of equations in terms of m_i can also be found.

For the two-dimensional Navier-Stokes equations, a spline ADI procedure has been used. This two-step method applies the spline procedure to each of the one-half step ADI equations. The cross derivatives are found by using equation (19) with the cross derivatives being m_i and the appropriate first derivatives replacing u_i. The three governing equations are solved sequentially at each row and column during the horizontal and vertical sweeps, respectively.

The boundary conditions for u_{xx}, u_{yy}, v_{xx}, v_{yy}, ρ_x, and ρ_y are found by evaluating the appropriate governing equation at the boundary with the time derivative set equal to zero, to give in effect steady-state boundary conditions. The initial values of the second derivatives of u and v and first derivatives of ρ are obtained by fitting cubic splines to the given initial function values.

COMPUTATIONAL RESULTS

Subsonic Boundary Conditions

One of the major difficulties associated with the computation of case 1 is proper specification of boundary conditions for the region of subsonic flow, i.e., for the subsonic portion of the inflow jet profile, the peripheral inflow, and the subsonic portion of the downstream boundary. This boundary-condition problem was therefore studied for case 2 with $N_{Re} = 8.1 \times 10^4$ using hopscotch as well as a second-order Du Fort-Frankel procedure described by Gottlieb and Gustafsson in reference 25.

The mathematical analysis of boundary-condition specification by Gottlieb and Gustafsson (ref. 12) formed the basis for this study. At the left subsonic inflow boundary (see fig. 4), the analysis indicated that two of the three dependent variables (u, v, and ρ) must be specified. Since v was itself a characteristic variable in the x-direction, it had to be one of the two specified functions; u was the logical choice for the second. The density boundary condition was chosen to be $\rho_x = 0$. No difficulties were encountered in any of the calculations with this set of inflow boundary conditions. At the upper inflow boundary, u is a characteristic variable in the y-direction; therefore, again u and v were specified and $\rho_y = 0$ was selected as the third boundary condition. This combination created no numerical difficulties in any calculations. However, the combination of ρ and u specified with $v_y = 0$ usually led to erroneous values for v, especially in the region near the upper boundary where positive values of v, indicating outflow, occurred.

At the subsonic outflow boundary the one-dimensional analysis indicated that one function value, either ρ or u, must be specified. Of course such a boundary condition is not convenient for most applications since downstream function values are generally not known a priori. Figure 5 shows the results of calculations using hopscotch with three different subsonic downstream boundary conditions. The boundary conditions used in the subsonic region are indicated in figure 4.

The initial flow field was obtained by setting the downstream (outflow) boundary values for u and v equal to one-half of their steady-state values (obtained from the parabolic code described in ref. 11) and linearly interpolating to obtain values at interior nodes. Computed steady-state profiles of the streamwise and normal velocity components u and v, respectively, at the downstream boundary are compared with results obtained with the parabolic technique. The streamwise component is accurately predicted for all three boundary conditions; however, only the specification of ρ gives a smooth and accurate v profile. Specifying u produces large oscillations in the v profile in the viscous region. These oscillations may be critical in turbulent flows when the turbulence model is locally a function of $\partial v/\partial y$. The least accurate results are obtained for linear extrapolation of all three function values.

The results of calculations with the Du Fort-Frankel procedure (see ref. 12) were identical to the hopscotch results with the exception that the linear extrapolation had to be altered to obtain converged solutions. Extrapolation of values at time level $n+1$ to obtain boundary values does not work for any degree of extrapolation (linear, quadratic, etc.). Linear extrapolation of the form

$$f_{i_{max},j}^{n+1} = 2f_{i_{max}-1,j}^{n} - f_{i_{max}-2,j}^{n-1} \tag{30}$$

for ρ, u, and v, where i_{max} is the outflow boundary, gave results which converged to the correct steady state. The boundary condition

$$f_{i_{max},j}^{n+1} = f_{i_{max}-1,j}^{n} \tag{31}$$

which has been shown to be stable for scalar hyperbolic equations for the pure leapfrog scheme in reference 26, also gave good results. Using both values at $n+1$ in equation (31) results in an unstable condition.

Parallel Mixing Calculations

Calculations of case 3 were made with the hopscotch and ADI methods for $N_{Re} = 10^3$ and 5×10^3. The supersonic inflow, supersonic outflow, and upper inflow boundary conditions shown in figure 4 were used. The computed steady state u and v velocity profiles and pressure profiles at $x = 0.15$ for $N_{Re} = 10^3$ are compared in figure 6 with the corresponding calculation using a parabolic method. The ADI and hopscotch results are virtually identical with both procedures accurately predicting u and v. For this grid spacing ($\Delta x = \Delta y = 0.025$), the pressure shows high-frequency oscillations in the viscous mixing region, although the maximum oscillation is only about 2 percent of the correct value. For the initial flow field the $y = 0$ inflow profiles were also specified at all other x-stations downstream. The time step in the hopscotch calculation was 0.9 of the maximum allowed for stability, i.e., the Courant number N_{Co} was 0.9. Identical solutions were also obtained with ADI for $N_{Co} = 6$ but with no decrease in the total number of steps to steady state. The solution diverged for $N_{Co} = 12$.

At both $N_{Co} = 6$ and 12, the large time step was used for the entire solution. The probable cause of divergence at $N_{Co} = 12$ is roundoff error from the tridiagonal matrix inversion occurring when the coefficient matrix did not possess diagonal dominance, a sufficient but not necessary condition for convergence of the matrix reduction. In this instance the continuity equation was not diagonally dominant for any row in the horizontal sweep, and in addition, the two momentum equations lacked diagonal dominance for many rows.

Figure 7 contains the steady-state results at $x = 0.15$ for $N_{Re} = 5.0 \times 10^3$. Figure 7(a) shows that again the hopscotch and ADI results are virtually identical for u and v. With the same grid spacing as in the previous calculation, u is accurately predicted, whereas the v profile exhibits an oscillation in the viscous region. Halving the grid so that $\Delta x = \Delta y = 0.0125$ eliminated this oscillation. The pressure profile shown in figure 7(b) has very small oscillations for both grids with the hopscotch pressure varying less from the constant value given by the parabolic code than the ADI pressure. For $N_{Co} = 0.8$, with either grid, the ADI method required approximately 5 times as many steps for convergence to steady state as hopscotch. The solution was considered to be converged when

$$\frac{f_{i,j}^{n+1} - f_{i,j}^{n}}{\Delta t} \leq 0.01\, g_{i,j}^{n} \qquad (32)$$

for $f = \rho$, u, and v at every point in the field and $g = \rho$, u, and u, respectively. Converged ADI solutions were obtained for $N_{Co} = 6$, but the solution again diverged for $N_{Co} = 12$. Hopscotch solutions were not attempted with Courant numbers significantly greater than one.

Figure 8 shows results of hopscotch calculations for case 3 with $N_{Re} = 8.1 \times 10^4$. Profiles of v and p are shown at the downstream boundary $x = 0.45$. The boundary conditions shown in figure 4 were used with function values obtained from the parabolic procedure providing the necessary specifications of v at the upper boundary and ρ at the downstream boundary. The initial field was obtained by using steady-state values of all functions (obtained from parabolic code) at the downstream boundary and calculating the interior values by linear interpolation. This gives an initial flow field which is a good approximation of the steady-state field. For a grid spacing of $\Delta x = \Delta y = 0.025$, the hopscotch solution converged in 1637 time steps. The u velocity component was accurately predicted, and figure 8 ($\alpha = 0$ curve) shows that v also agreed with the parabolic results; however, small oscillations occurred in the pressure. It was found that the pressure could be smoothed by explicitly adding artificial diffusion to the continuity equation, that is,

$$\rho_t + (\rho u)_x + (\rho v)_y = \alpha(\Delta x)^2 \rho_{xx} + \alpha(\Delta y)^2 \rho_{yy} \tag{33}$$

Victoria and Widhopf (ref. 27) also found it necessary to add artificial diffusion to the continuity equation. For this case, $\alpha = 0.1$ smoothed the pressure without altering u or v; moreover, the solution converged in 1150 time steps. (The coefficient of ρ_{xx} is then approximately 5 to 10 times as large as the average coefficients of the viscous terms in the two momentum equations.) Although the solution converged in 1837 time steps for $\alpha = 1.0$, both p and v show oscillations. For $\alpha = 0$, a significantly different initial flow field was generated by halving u and v at the downstream edge and then linearly interpolating for interior values. Steady state was reached in 3050 steps with u, v, and p found to be identical to the previous results. For this grid, no converged ADI results were obtained with or without artificial diffusion. Oscillations in v in the mixing region grew with time, and the solution diverged.

The Du Fort-Frankel procedure with the downstream boundary condition given by equation (31) for u and v was compared with hopscotch which used linear extrapolation when the initial flow field was obtained by setting the outflow values of u and v to one-half of their steady-state values and linearly interpolating for interior values. Both solutions converged to steady state at approximately the same nondimensional time, although slightly different time steps were used in each method. The maximum difference in the u profiles was approximately 3 percent and occurred in the viscous region. This slight difference is attributed to the difference in explicit artificial diffusion in the two methods. Second-order diffusion with $\alpha = 0.1$ was used in hopscotch, and fourth-order diffusion was added to the Du Fort-Frankel procedure.

Results for Case 1

Computations were attempted for the original test problem, case 1, with a Reynolds number of 8.1×10^4 with the two finite-difference methods and with the finite-element method. A nonuniform grid was used for the finite-difference methods. From the sharp corner, Δy was increased by a factor of 1.05 for each successive spacing in the positive and negative y-directions from the smallest value, $\Delta y = 0.005$. Thus, grid points were concentrated in the viscous mixing region. The grid also increased in the x-direction by a factor of 1.05 $\left(\Delta x_i / \Delta x_{i-1} = 1.05\right)$ for each successive spacing.

Computations with hopscotch were made with the boundary conditions of figure 4 along with a no-slip wall condition and constant density assumption near the wall. The upper boundary was approximately six jet diameters above the center line. Figure 9 shows steady-state hopscotch results for an interior x-location using linear extrapolation for density in the subsonic portion of the outflow boundary (extrapolation used since ρ is unknown). The magnitude of the peripheral velocity at the upper boundary was 0.07, which is several times greater than the natural entrainment for the same jet issuing into still air. Since the upper boundary effectively models a porous wall with nonuniform mass injestion into the boundary layer, it was necessary to modify the upper boundary conditions by setting $u_y = 0$. The results shown in figure 9 were obtained with $\alpha = 10$ after 3 hr of computing time on a CDC 6600 computer. As expected from the parallel mixing results, the u component is smooth and appears to be qualitatively correct. (There are no known experimental data for such a flow with which to compare the computed results.) The v profile shows the oscillation characteristic of using linear extrapolation for the subsonic outflow density. For some engineering applications, however, these results may be sufficient. The local increase in the pressure profile indicates the presence of a weak shock.

Fully converged ADI results were not obtained for case 1. With linear density extrapolation and the same nonuniform grid, the solutions appeared to be nearly converged after approximately 3 hr of CPU time on the CDC 6600, but the computations were not continued further since the results did not appear to be better than hopscotch. As with hopscotch, the u profiles were smooth and apparently qualitatively correct, although v again exhibited spatial oscillations.

At the present time, converged results have not been obtained with the finite-element method for this problem. The major difficulties appear to be the lack of sufficient spatial resolution in the viscous region and incorporation of the second-derivative downstream continuation boundary conditions. The 103-triangle mesh currently in use (shown in fig. 3) requires excessive machine storage and prohibits a significant increase in resolution.

The cubic spline algorithm has been coded, but presently no steady-state results have been obtained.

CODE COMPARISON

For case 1 the hopscotch code requires machine storage of approximately 50000_8 for 3045 node points, whereas the ADI method requires approximately 150000_8 for the same grid. The 103-triangle finite-element mesh which has 301 nodes requires 330000_8. The cubic spline algorithm will presumably require fewer grid points for accuracy comparable to the finite-difference results.

For each Δt step the CPU time on the CDC 6600 for hopscotch is 1.08×10^{-3} sec/node and for the ADI method, 3.74×10^{-3} sec/node. The finite-element code requires 1.93×10^{-1} sec/node to assemble the matrices and even with the fast block iterative solver, requires 4.25×10^{-2} sec/node for equation solution at each time step. No data are available for the spline code. (The Du Fort-Frankel code requires 1.28×10^{-3} sec/node for each time step.)

CONCLUDING REMARKS

A study of mixed supersonic-subsonic free shear flows has shown that correct calculation of the normal velocity component required specification of the density in the subsonic portion of the outflow boundary. The streamwise velocity was, however, correctly computed even when linear density extrapolation was used for this boundary.

For high Reynolds number flows (flows with small viscous terms in the momentum equations), it was necessary to add artificial diffusion in the continuity equation to eliminate oscillations in the static pressure. The addition of too much artificial viscosity had adverse effects on both the pressure and the normal component of velocity.

For the problems considered, the maximum allowable time step for the sequential alternating-direction implicit (ADI) procedure was less than 10 times the maximum explicit time step. This increase in time step, however, did not significantly improve the convergence rate. The hopscotch procedure, with a time step no greater than the maximum explicit time step, still converged faster than any of the ADI solutions. A fully coupled ADI procedure may allow larger time steps; however, the effect of large steps on convergence rate must be investigated.

The finite-element method with cubic elements appears to have excessive storage requirements and computing times. Therefore, as currently formulated, it does not appear to be a competitive procedure for high Reynolds number calculations in aerospace vehicle analysis.

REFERENCES

1. Peyret, Roger; and Viviand, Henri: Numerical Solution of the Navier-Stokes Equations for Compressible Fluids. ONERA T.P. No. 1319, 1973.

2. Taylor, T. D.: Numerical Methods for Predicting Subsonic, Transonic, and Supersonic Flow. AGARDograph No. 187, Jan. 1974.

3. Briley, W. R.; and McDonald, H.: An Implicit Numerical Method for the Multidimensional Compressible Navier-Stokes Equations. Rep. M911363-6 (Contract No. N00014-72-C-0183), United Aircraft Res. Lab., United Aircraft Corp., Nov. 1973. (Available from DDC as AD 770 224.)

4. Baum, Eric; and Ndefo, Ejike: A Temporal ADI Computational Technique. AIAA Computational Fluid Dynamics Conference, July 1973, pp. 133-140.

5. Victoria, Keith J.; and Steiger, Martin H.: Exact Solution of the 2-D Laminar Near Wake of a Slender Body in Supersonic Flow at High Reynolds Number. IAF Paper 55, Oct. 1970.

6. Carter, James E.: Numerical Solutions of the Navier-Stokes Equations for the Supersonic Laminar Flow Over a Two-Dimensional Compression Corner. NASA TR R-385, 1972.

7. MacCormack, Robert W.: The Effect of Viscosity in Hypervelocity Impact Cratering. AIAA Paper No. 69-354, Apr.-May 1969.

8. Holst, T. L.; and Tannehill, J. C.: Numerical Computation of Two-Dimensional Viscous Blunt Body Flows With an Impinging Shock. NASA CR-138594, 1974.

9. Baldwin, B. S.; and MacCormack, R. W.: Numerical Solution of the Interaction of a Strong Shock Wave With a Hypersonic Turbulent Boundary Layer. AIAA Paper No. 74-558, June 1974.

10. Holst, Terry L.; Tannehill, John C.; and Rakich, John V.: Numerical Computation of Viscous Blunt Body Flows With a Planar Impinging Shock. Aerodynamic Analyses Requiring Advanced Computers, Part II, NASA SP-347, 1975, pp. 1457-1471.

11. Oh, Y. H.: Analysis of Two-Dimensional Free Turbulent Mixing. AIAA Paper No. 74-594, June 1974.

12. Gottlieb, David; and Gustafsson, Bertil: On the Navier-Stokes Equations With Constant Total Temperature. NASA CR-132664, 1975.

13. Gourlay, A. R.: Hopscotch: A Fast Second-Order Partial Differential Equation Solver. J. Inst. Math. & Its Appl., vol. 6, no. 4, Dec. 1970, pp. 375-390.

14. Scala, Sinclaire M.; and Gordon, Paul: Solution of the Time-Dependent Navier-Stokes Equations for the Flow Around a Circular Cylinder. AIAA J., vol. 6, no. 5, May 1968, pp. 815-822.

15. Gourlay, A. R.; and Morris, J. Ll.: Hopscotch Difference Methods for Nonlinear Hyperbolic Systems. IBM J. Res. & Develop., vol. 16, no. 4, July 1972, pp. 349-353.

16. Peaceman, D. W.; and Rachford, H. H., Jr.: The Numerical Solution of Parabolic and Elliptic Differential Equations. J. Soc. Ind. & Appl. Math., vol. 3, no. 1, Mar. 1955, pp. 28-41.

17. Von Rosenburg, Dale U.: Methods for the Numerical Solution of Partial Differential Equations. American Elsevier Pub. Co., Inc., 1969.

18. Gourlay, A. R.; and Mitchell, A. R.: Alternating Direction Methods for Hyperbolic Systems. Numer. Math., Bd. 8, Heft 2, Apr. 4, 1966, pp. 137-149.

19. Polezhaev, V. I.: Numerical Solution of the System of Two-Dimensional Unsteady Navier-Stokes Equations for a Compressible Gas in a Closed Region. Fluid Dyn., vol. 2, no. 2, Mar.-Apr. 1967, pp. 70-74.

20. Norrie, Douglas H.; and De Vries, Gerard: The Finite Element Method. Academic Press, Inc., 1973.

21. Baker, A. J.: A Finite Element Solution Algorithm for the Navier-Stokes Equations. NASA CR-2391, 1974.

22. Douglas, Jim, Jr.; and Dupont, Todd: Galerkin Methods for Parabolic Equations. SIAM J. Numerical Anal., vol. 7, no. 4, Dec. 1970, pp. 575-626.

23. Rubin, Stanley G.; and Graves, Randolph A., Jr.: A Cubic Spline Approximation for Problems in Fluid Mechanics. NASA TR R-436, 1975.

24. Crowder, H. J.; and Dalton, C.: Errors in the Use of Nonuniform Mesh Systems. J. Comput. Phys., vol. 7, no. 1, Feb. 1971, pp. 32-45.

25. Gottlieb, David; and Gustafsson, Bertil: Generalized Du Fort-Frankel Methods for Parabolic Initial-Boundary-Value Problems. NASA CR-132653, 1975.

26. Gustafsson, Bertil; Kreiss, Heinz-Otto; and Sundström, Arne: Stability Theory of Difference Approximations for Mixed Initial Boundary Value Problems. II. Math. Comput., vol. 26, no. 119, July 1972, pp. 649-686.

27. Victoria, Keith J.; and Widhopf, George F.: Numerical Solution of the Unsteady Navier-Stokes Equations in Curvilinear Coordinates: The Hypersonic Blunt Body Merged Layer Problem. Proceedings of the Third International Conference on Numerical Methods in Fluid Mechanics, Volume II. Volume 19 of Lecture Notes in Physics, Henri Cabannes and Roger Teman, eds., Springer-Verlag, 1973, pp. 254-267.

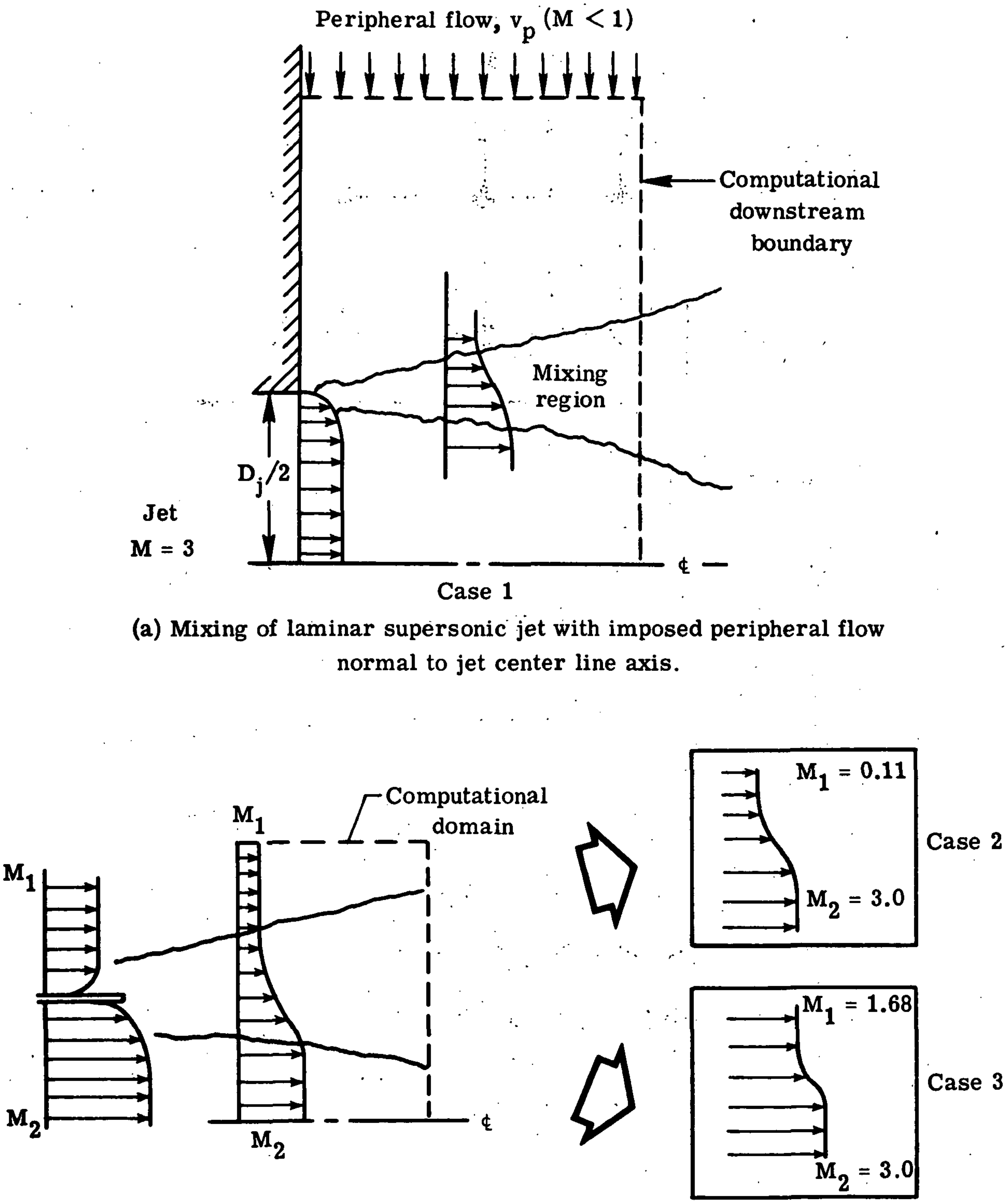

(a) Mixing of laminar supersonic jet with imposed peripheral flow normal to jet center line axis.

(b) Mixing of two parallel flows.

Figure 1.- Standard sample problems.

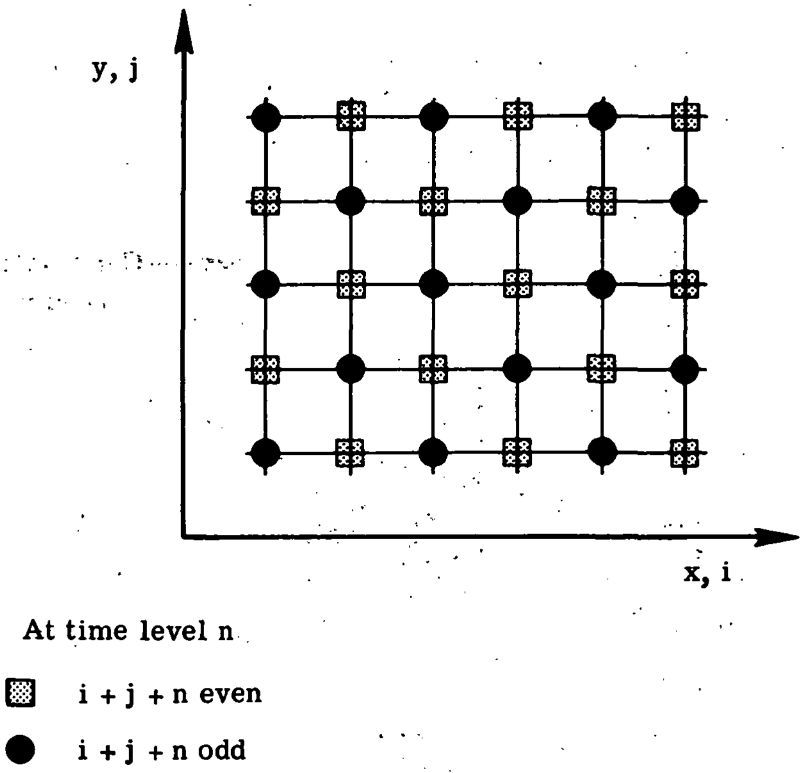

Figure 2.- Hopscotch grid.

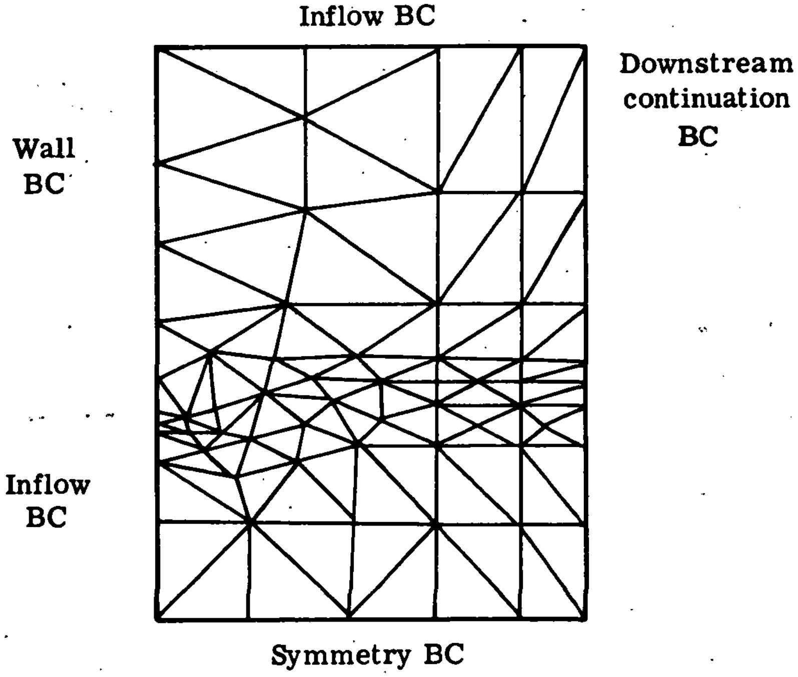

Figure 3.- Solution domain showing finite-element mesh for case 1 with 103 triangles with boundary conditions (BC) indicated.

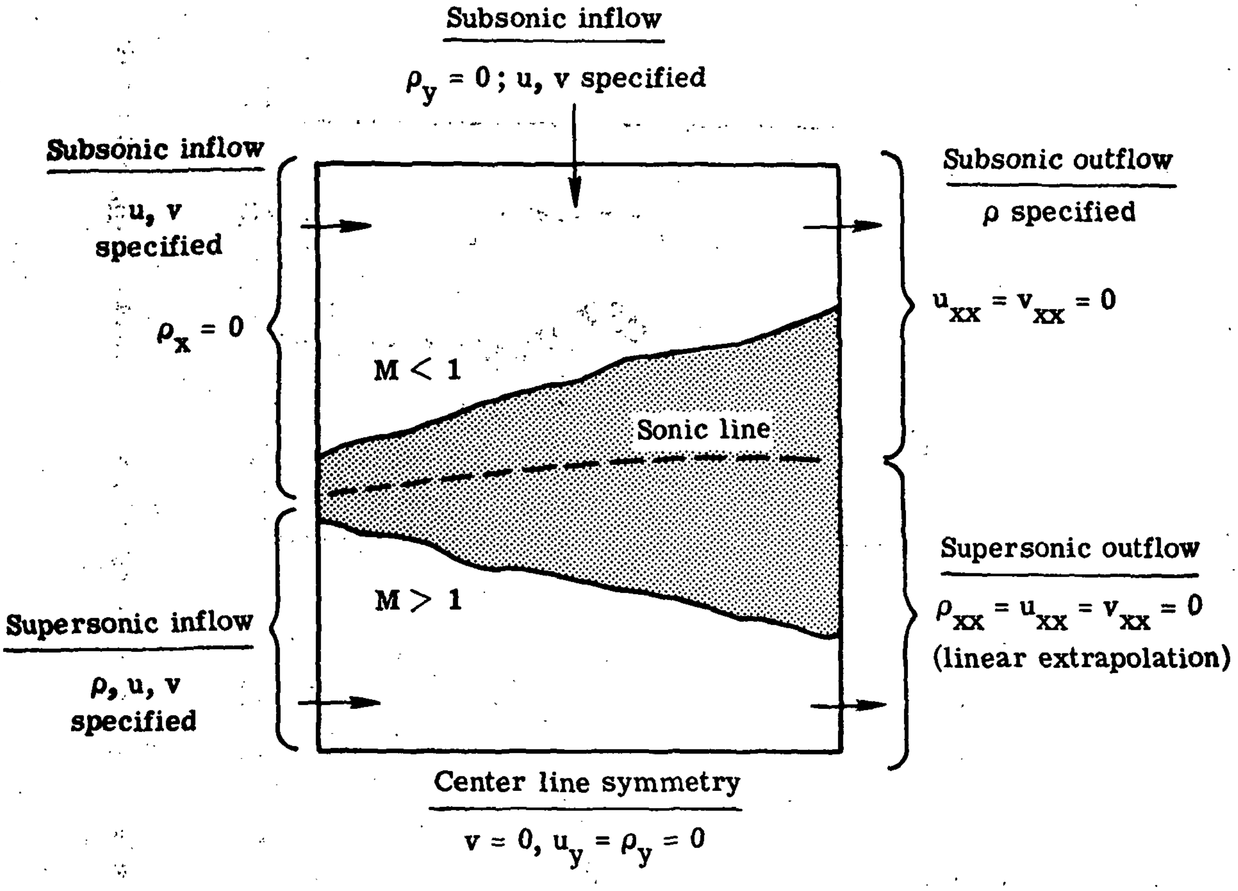

Figure 4.- Schematic of computational domain with best boundary conditions for case 2.

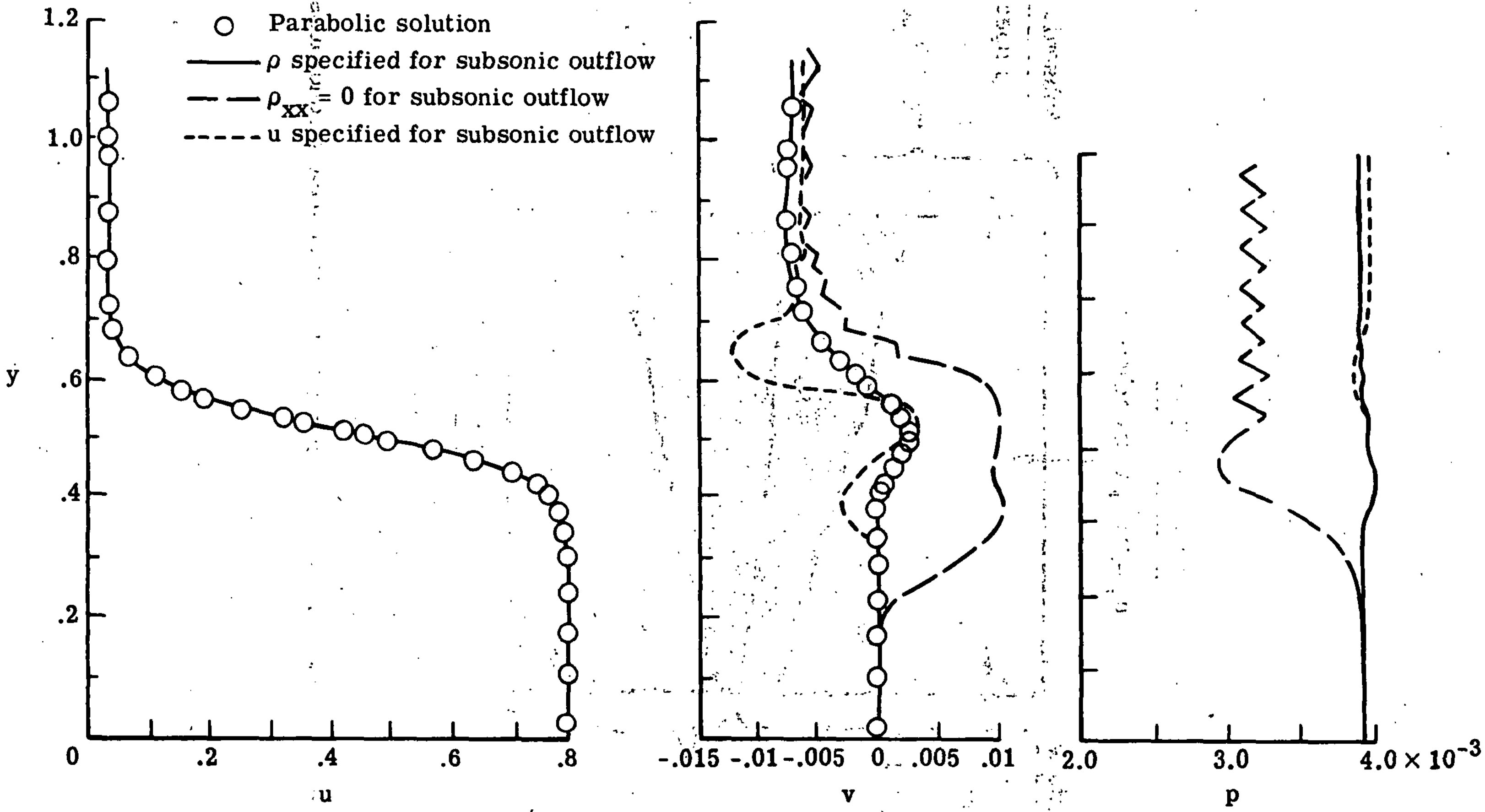

Figure 5.- Boundary-condition study for subsonic boundary. $N_{Re} = 8.1 \times 10^4$; x = 0.45.

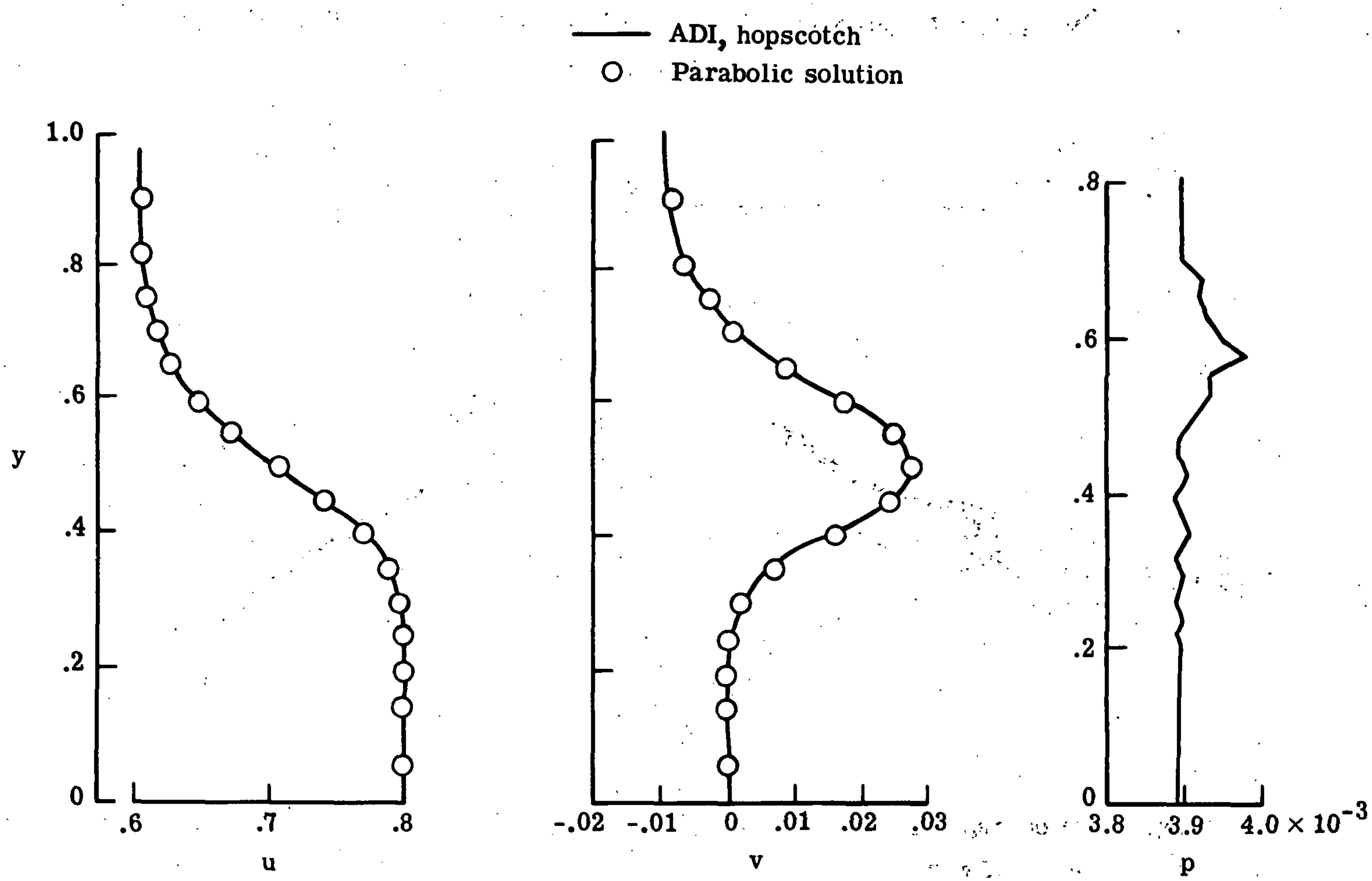

Figure 6.- Supersonic-supersonic mixing for $N_{Re} = 10^3$; $\Delta x = \Delta y = 0.025$; $N_{Co} = 0.9$.

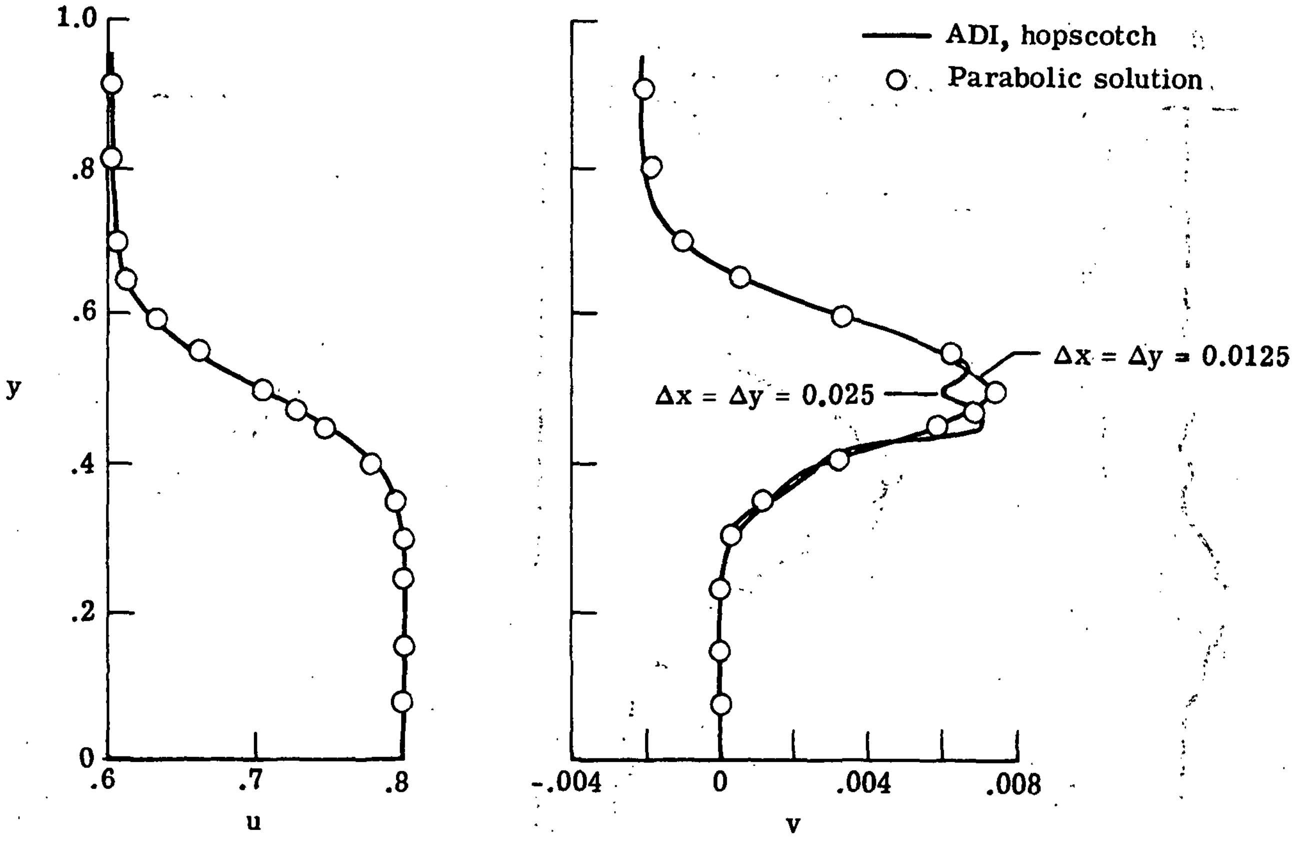

(a) Velocity profiles.

Figure 7.- Subsonic-supersonic mixing for $N_{Re} = 5 \times 10^3$. $x = 0.15$; $N_{Co} = 0.9$.

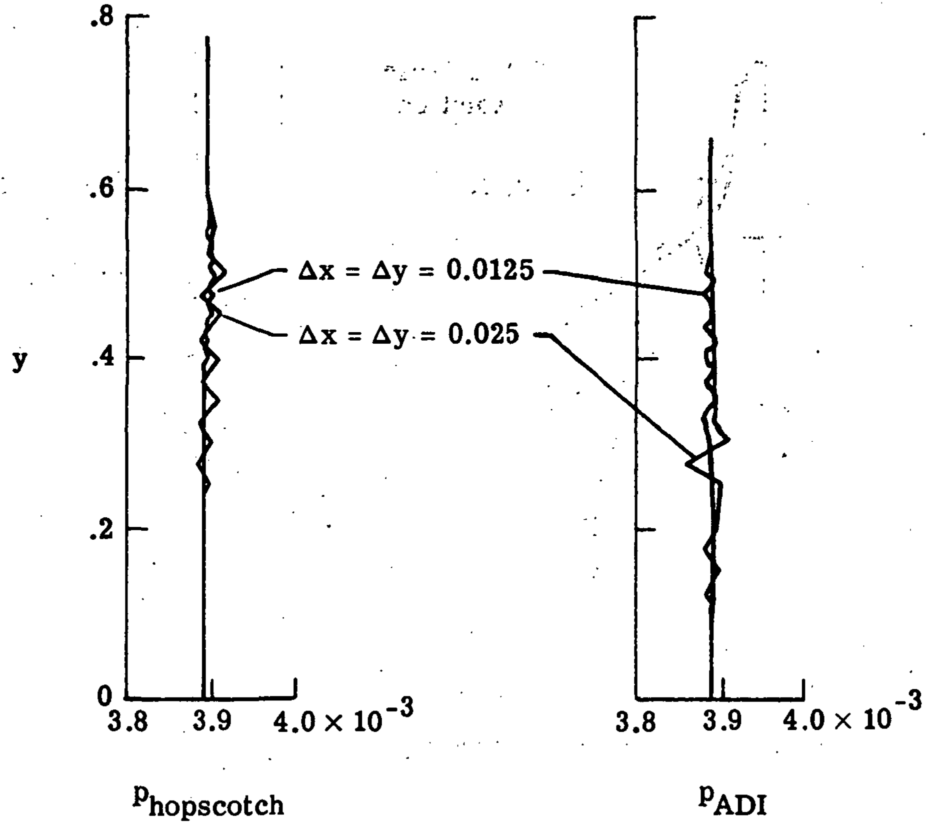

(b) Pressure profiles.

Figure 7.- Concluded.

$$\rho_t + (\rho u)_x + (\rho v)_y = (\Delta x)^2 \alpha \rho_{xx} + (\Delta y)^2 \alpha \rho_{yy}$$

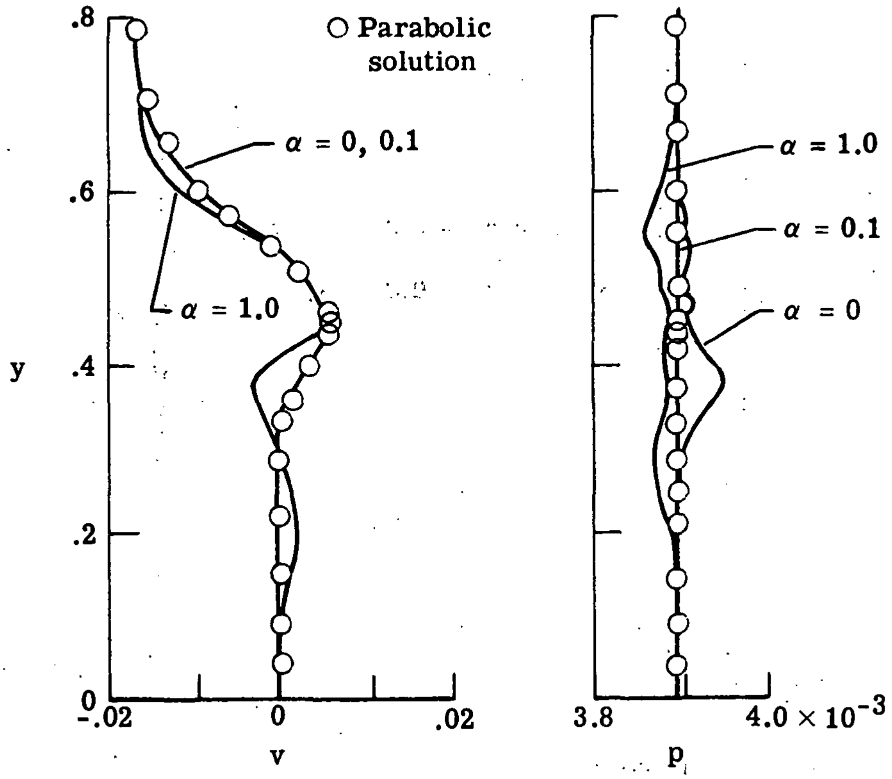

Figure 8.- Effect of artificial diffusion in continuity equation. $N_{Re} = 8.1 \times 10^4$; x = 0.45.

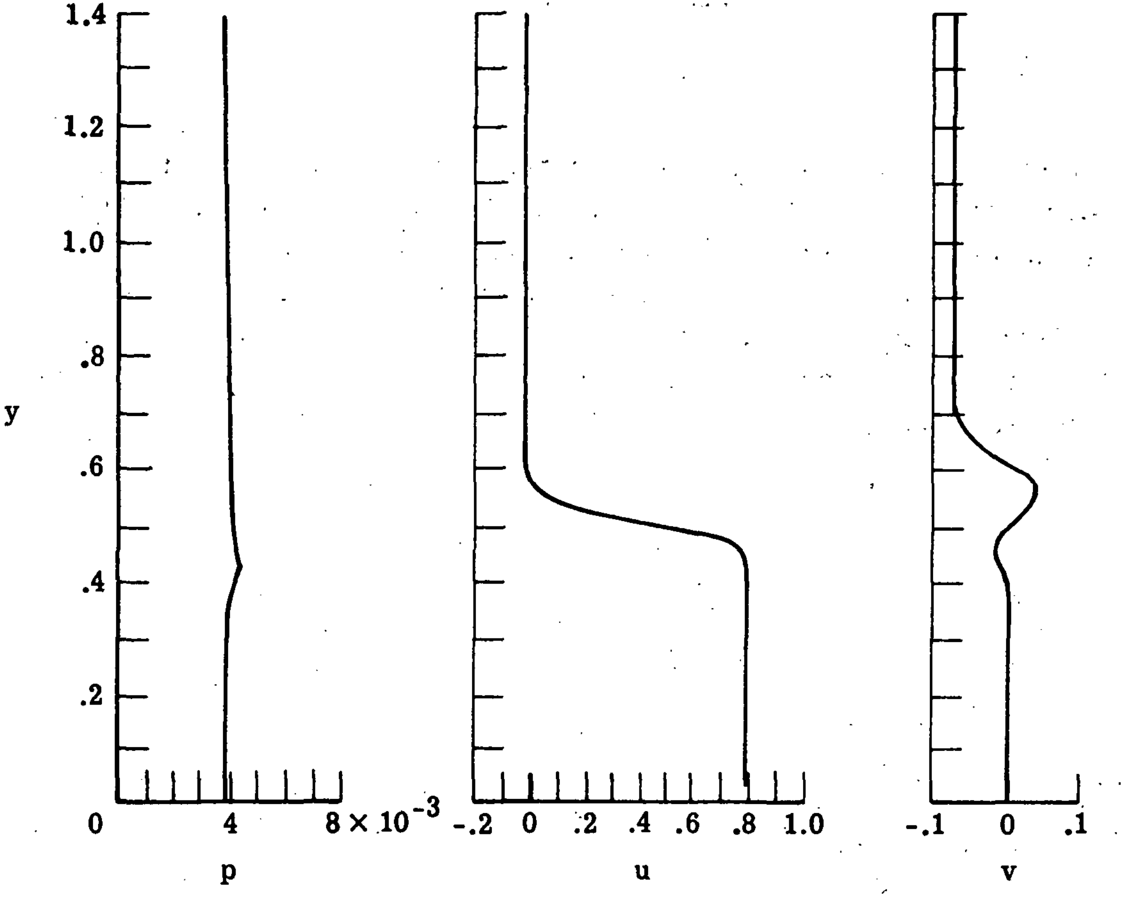

Figure 9.- Steady-state hopscotch results for case 1 with peripheral velocity of -0.07. $N_{Re} = 8.1 \times 10^4$; $x = 0.367$; $\alpha = 10$.